Thermal evolution of permeability and microstructure in sea ice

K. M. Golden,[1] H. Eicken,[2] A. L. Heaton,[1] J. Miner,[2] D. J. Pringle,[2,3] and J. Zhu[1]

Received 20 April 2007; accepted 27 June 2007; published 16 August 2007.

[1] The fluid permeability k of sea ice constrains a broad range of processes, such as the growth and decay of seasonal ice, the evolution of summer ice albedo, and biomass build-up. Such processes are critical to how sea ice and associated ecosystems respond to climate change. However, studies of k and its dependence on brine porosity ϕ and microstructure are sparse. Here we present a multifaceted theory for $k(\phi)$ which closely captures laboratory and field data. X-ray computed tomography provides an unprecedented look at the brine phase and its connectivity. We find that sea ice displays universal transport properties remarkably similar to crustal rocks, yet over a much narrower temperature range. Our results yield simple parameterizations for fluid transport in terms of temperature and salinity, and permit more realistic representations of sea ice in global climate and biological models. **Citation:** Golden, K. M., H. Eicken, A. L. Heaton, J. Miner, D. J. Pringle, and J. Zhu (2007), Thermal evolution of permeability and microstructure in sea ice, *Geophys. Res. Lett.*, *34*, L16501, doi:10.1029/2007GL030447.

1. Introduction

[2] Polar sea ice is a critical component of earth's climate system, both as an indicator and agent of climatic change [*Serreze et al.*, 2007; *Thomas and Dieckmann*, 2003]. It is also a primary habitat for microbial communities which sustain the rich foodwebs of the polar oceans [*Thomas and Deickmann*, 2003; *Fritsen et al.*, 1994]. The geophysical and biological importance of sea ice is largely derived from its porous composite structure [*Thomas and Dieckmann*, 2003; *Weeks and Ackley*, 1986]. Pivotal to understanding and predicting the behavior of sea ice in the environment is its permeability k, which controls bulk flow and depends on the fluid volume fraction ϕ and microstructural characteristics. Brine transport facilitates sea ice production from freezing of flooded ice surfaces, convection-enhanced thermal transport, and the input of brine and fresh water into the upper ocean from freezing, melting, and drainage processes [*Weeks and Ackley*, 1986; *Thomas and Dieckmann*, 2003]. For example, summer sea-ice albedo, a key parameter in the global climate system, depends on surface melt-pond hydrology whose evolution is controlled largely by ice permeability [*Eicken et al.*, 2004]. The transport of nutrients and enzymes through the pore matrix of sea ice is essential for sustaining life in this extreme environment [*Thomas and Dieckmann*, 2003; *Fritsen et al.*, 1994]. Furthermore, through its control of the presence and nature of liquid water at the ice surface, $k(\phi)$ is a key variable in sea-ice remote sensing, a principal tool for monitoring global warming.

[3] Yet, despite its importance, the problem of understanding how k depends on the brine microstructure has received relatively little attention [*Thomas and Dieckmann*, 2003; *Eicken et al.*, 2004; *Golden et al.*, 1998; *Petrich et al.*, 2006; *Wettlaufer et al.*, 1997; *Oertling and Watts*, 2004; *Ono and Kasai*, 1985; *Freitag*, 1999]. Here we address this fundamental issue theoretically, using rigorous bounds, percolation and hierarchical models, and numerical simulation, and experimentally with laboratory and Arctic field data on $k(\phi)$, obtaining close agreement. We also develop micro-scale imaging methods based on X-ray computed tomography (CT) and pore structure analysis [*Prodanovic et al.*, 2006] to provide detailed pictures of the brine microstructure and its evolution with temperature, along with quantitative measurements of 3-D pore connectivity. Our microstructural imaging results support the theory and help to interpret the permeability data. Moreover, they illuminate important deviations from the classic sea-ice microstructural model [*Thomas and Dieckmann*, 2003; *Weeks and Ackley*, 1986], and provide the first direct, quantitative evidence for a transition in connectedness which was conjectured [*Golden et al.*, 1998] nearly a decade ago.

[4] It has long been observed [*Weeks and Ackley*, 1986] that columnar sea ice is effectively impermeable to brine transport for ϕ less than about 5%, yet is permeable for ϕ above 5%. For a bulk salinity S of 5 parts per thousand (ppt), the critical porosity $\phi_c \approx 5\%$ corresponds to a critical temperature $T_c \approx -5°\mathrm{C}$, via equations relating ϕ to T and S [*Thomas and Dieckmann*, 2003; *Weeks and Ackley*, 1986]. This rule of fives was discussed [*Golden et al.*, 1998] in terms where ϕ_c was identified with the critical probability in a continuum percolation model for a compressed powder [*Kusy and Turner*, 1971] exhibiting microstructural characteristics qualitatively similar to sea ice. In percolation theory, the permeability just above a threshold can be characterized by a critical exponent e and a scaling factor. In the continuum, e can vary depending on local properties, yet for lattice systems it is believed to be universal, depending only on dimension [*Torquato*, 2002; *Halperin et al.*, 1985]. Here we find the striking result that for sea ice, $e \approx 2$, the universal lattice value in three dimensions [*Torquato*, 2002; *Golden*, 1990], due to the general lognormal structure of the brine inclusion distribution function [*Perovich and Gow*, 1996]. The general nature of our results suggests that similar types of porous media, such as saline ice on extraterrestrial bodies [*Thomas and Dieckmann*, 2003] may also exhibit universal critical behavior.

[1] University of Utah, Department of Mathematics, Salt Lake City, Utah, USA.
[2] Geophysical Institute, University of Alaska Fairbanks, Fairbanks, Alaska, USA.
[3] Arctic Region Supercomputing Center, University of Alaska Fairbanks, Fairbanks, Alaska, USA.

0094-8276/07/2007GL030447$05.00

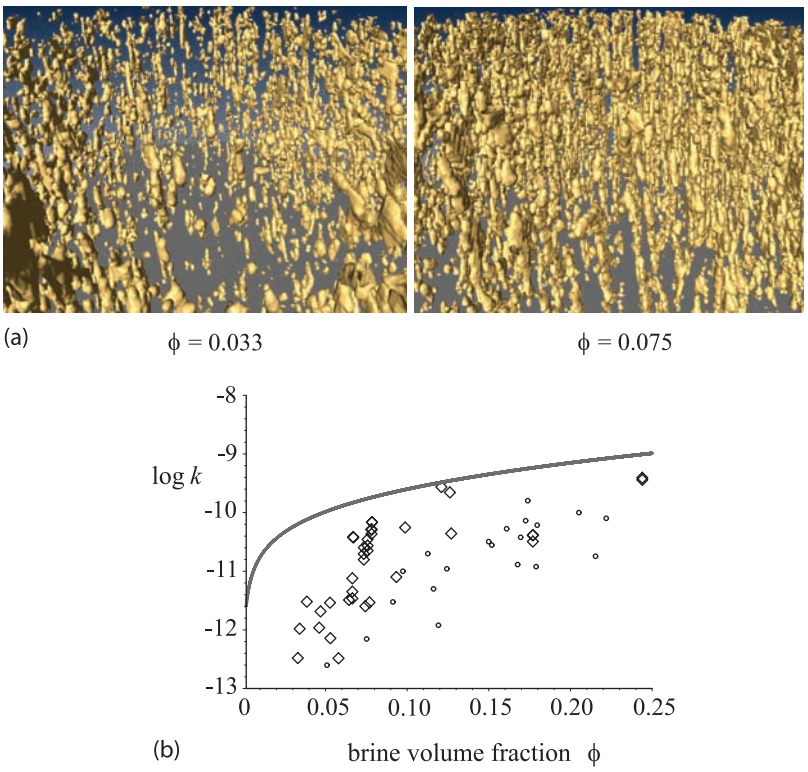

Figure 1. (a) X-ray CT images ($\approx$ 10 mm across) of the brine microstructure of sea ice for two values of the porosity ϕ. As temperature and ϕ increase, so do inclusion sizes and connectivity. (b) Comparison of in situ data on k (m^2) for Arctic sea ice (37 diamonds) and lab data [*Freitag*, 1999] for artificially grown sea ice (20 circles) with the upper bound in (2).

[5] In fact, we find that the parameters characterizing fluid transport in sea ice are almost the same as in some crustal, sedimentary rocks [*Knackstedt and Cox*, 1995]. Both types of media exhibit critical behavior near a percolation threshold, with $\phi_c \approx 5\%$ for sea ice, and $\phi_c \approx 4\%$ for calcite aggregates and Fontainebleau sandstone. Moreover, even though the porous microstructures in these rocks are quite different from sea ice, the permeability critical exponent in both cases falls into the lattice universality class. Another permeability exponent discussed below is also about the same in both cases. It is interesting to note that a variation of four orders of magnitude in the permeability of calcite aggregates [*Knackstedt and Cox*, 1995] is achieved with temperatures ranging from 633 K to 833 K, and with confining pressures from 200 MPa to 300 MPa. For the in situ sea ice data considered here, a similar variation in permeability occurs over a temperature range of about 15 K.

2. Results

[6] We consider low Reynolds number flow of brine of viscosity η through sea ice. The volume fractions of brine and ice are ϕ and $1 - \phi$. The velocity and pressure fields in the brine satisfy the Stokes equations for incompressible fluids. Under appropriate assumptions [*Torquato*, 2002], the homogenized velocity $\mathbf{v}(\mathbf{x})$ and pressure $p(\mathbf{x})$ satisfy Darcy's law $\mathbf{v} = -\mathbf{k}\nabla p/\eta$ and $\nabla \cdot \mathbf{v} = 0$, where $\mathbf{k}$ is the permeability tensor, with vertical permeability $k_{zz} = k$ in units of m^2. Transport depends on pore-size statistics, and in sea ice the inclusion cross-sectional areas A (above a cut-off) are lognormally distributed [*Perovich and Gow*, 1996]. Then $Z = \ln A$ has a normal probability density with mean μ and variance σ^2,

$$P(Z) = \frac{1}{\sqrt{2\pi\sigma^2}} e^{-(Z-\mu)^2/2\sigma^2}. \quad (1)$$

[7] The bulk of sea-ice brine resides in intra-crystalline layers whose connectivity is expected to underpin the development of larger-scale permeability. As a first step to obtain quantitative information about pore connectivity across all relevant scales, we tracked the thermal evolution of the connectivity of the intragranular inclusions from X-ray CT of laboratory-grown sea-ice single crystals [*Pringle et al.*, 2006] (doped with CsCl to improve ice/brine contrast), as shown in Figure 1a (J. Miner et al., manuscript in preparation, 2007).

[8] Rigorous bounds on bulk properties of composites provide benchmarks which are useful in assessing data, and in connecting effective behavior to mixture geometry [*Torquato*, 2002]. In previous work [*Golden et al.*, 2006] we found a pipe bound, $k \leq \phi\, a^2(\phi)/8$ for porous media with uniformly sized inclusions, where the cross-sectional radius $a(\phi) = 7 \times 10^{-5} + (1.6 \times 10^{-4})\phi$ m increases according to measurements of pore sizes with temperature [*Perovich and Gow*, 1996; *Bock and Eicken*, 2005]. The pipe bound is a special case of optimal void bounds [*Torquato and Pham*, 2004; *Torquato*, 2002], and captures data on k for centrifuged cores of artificially grown sea ice [*Freitag*, 1999; *Golden et al.*, 2006]. However, when compared with in situ

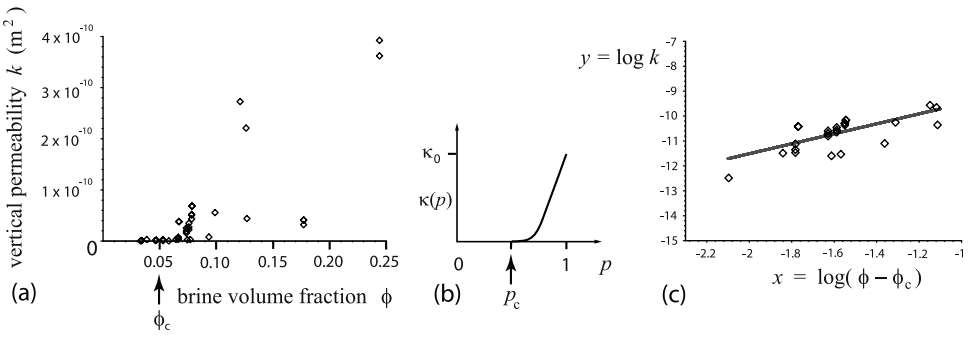

Figure 2. (a) Data for k taken in situ on Arctic sea ice, displayed on a linear scale. (b) The effective permeability $\kappa(p)$ in a lattice percolation model, displayed on a linear scale. (c) Comparison of Arctic permeability data in the critical regime (25 data points) with percolation theory in (4). In logarithmic variables the predicted line has the equation $y = 2\,x - 7.5$, while a best fit of the data yields $y = 2.07\,x - 7.45$, assuming [*Golden et al.*, 1998; *Petrich et al.*, 2006] $\phi_c = 0.05$.

data on Arctic sea ice with more microstructural variations and larger pores, often found in the form of vertical arrays or channels, some data exceed the bound.

[9] Here we evaluate the more general void bounds [*Torquato and Pham*, 2004] $k \leq \frac{\phi}{8}\langle R^4\rangle/\langle R^2\rangle$ for the lognormal distribution of brine inclusion cross sectional areas $A = \pi R^2$ in (1). Since $\ln A^2 = 2 \ln A$ is normally distributed with mean 2μ and variance $4\sigma^2$, a short calculation yields

$$k(\phi) \leq \frac{\phi}{8\pi}\langle A(\phi)\rangle e^{\sigma^2}. \tag{2}$$

With variance [*Perovich and Gow*, 1996] $\sigma^2 \approx 1$ and $\langle A(\phi)\rangle = \pi a^2(\phi)$ as above, the lognormal pipe bound in (2) captures the field data, as well as the lab data, as shown in Figure 1b. The field data were taken near Barrow, Alaska in a hydrological bail test [*Freitag and Eicken*, 2004; *Eicken et al.*, 2004]. A cylindrical hole is drilled, a tube is inserted to seal off horizontal flow, and time series measurements of the water level are used to estimate the permeability of the ice under the hole. The total error for the derived permeability is estimated at < 50% for both the lab and field measurements, with significantly less relative error. The ϕ values for the lab data are effective porosities [*Freitag*, 1999; *Petrich et al.*, 2006]. For the range considered (except one point), the effective porosity differs only negligibly from the total porosity [*Petrich et al.*, 2006]. Viscosity estimates for pure brine are reasonably well constrained, with uncertainties an order of magnitude smaller than those for permeability. Organic polymers, such as those released from sea-ice microorganisms, may increase brine viscosity. While the impact on the relationships derived here is deemed of lower order, parameterizations of brine viscosity may need to take the presence of polymers into account. The result in (2) provides bounds on the trapping constant and mean survival time for diffusion which can react with the pore boundaries [*Torquato*, 2002; *Golden et al.*, 2006; *Torquato and Pham*, 2004]. Such processes arise in bacterial foraging and NMR imaging [*Torquato*, 2002; *Golden et al.*, 2006; *Bock and Eicken*, 2005].

[10] Percolation theory [*Torquato*, 2002; *Halperin et al.*, 1985; *Golden*, 1990] has been used to model disordered materials where the connectedness of one phase dominates effective behavior. Consider the square ($d = 2$) or cubic ($d = 3$) network of bonds joining nearest neighbor sites on the integer lattice $\mathbb{Z}^d$. The bonds are assigned fluid conductivities $\kappa_0 > 0$ (open) or 0 (closed) with probabilities p and $1 - p$. There is a critical probability p_c, $0 < p_c < 1$, called the percolation threshold, where an infinite, connected set of open bonds first appears. In $d = 2$, $p_c = \frac{1}{2}$, and in $d = 3$, $p_c \approx 0.25$. Let $\kappa(p)$ be the permeability of this random network in the vertical direction. For $p < p_c$, $\kappa(p) = 0$. For $p > p_c$, near the threshold $\kappa(p)$ exhibits power law behavior,

$$\kappa(p) \sim \kappa_0(p - p_c)^e, \qquad p \to p_c^+, \tag{3}$$

where e is the permeability critical exponent. For lattices, e is believed to be universal, depending only on d, and is equal to t, the lattice electrical conductivity exponent [*Torquato*, 2002; *Halperin et al.*, 1985; *Golden*, 1990; *Berkowitz and Balberg*, 1992]. In $d = 3$, it is believed [*Torquato*, 2002] that $t \approx 2.0$, and there is a rigorous bound [*Golden*, 1990] that $t \leq 2$.

[11] In the continuum, e can take non-universal values, such as for the three dimensional Swiss cheese model [*Torquato*, 2002; *Halperin et al.*, 1985; *Berkowitz and Balberg*, 1992]. Continuum models have been studied [*Torquato*, 2002; *Halperin et al.*, 1985; *Berkowitz and Balberg*, 1992] by mapping to a lattice with a probability density $\psi(g)$ of bond conductances g. Non-universal behavior can be obtained when $\psi(g)$ is singular as $g \to 0^+$. However, for a lognormal conductance distribution arising from intersections of lognormally distributed inclusions, as in sea ice, the behavior is universal, which has been verified numerically [*Berkowitz and Balberg*, 1992]. Thus $e \approx 2$ for sea ice.

[12] We estimate the scaling factor k_0 for sea ice using critical path analysis [*Friedman and Seaton*, 1998; *Golden and Kozlov*, 1999]. For media with g in a wide range, the overall behavior is dominated by a critical, bottleneck conductance g_c, the smallest conductance such that the critical path $\{g\colon g \geq g_c\}$ spans the sample. With most brine channel diameters [*Weeks and Ackley*, 1986] between 1.0 mm and 1.0 cm, spanning fluid paths have a smallest, characteristic radius $r_c \approx 0.5$ mm, and we estimate k_0 by the pipe-flow result $r_c^2/8$. Thus

$$k(\phi) \sim 3(\phi - \phi_c)^2 \times 10^{-8}\ \mathrm{m}^2, \qquad \phi \to \phi_c^+. \tag{4}$$

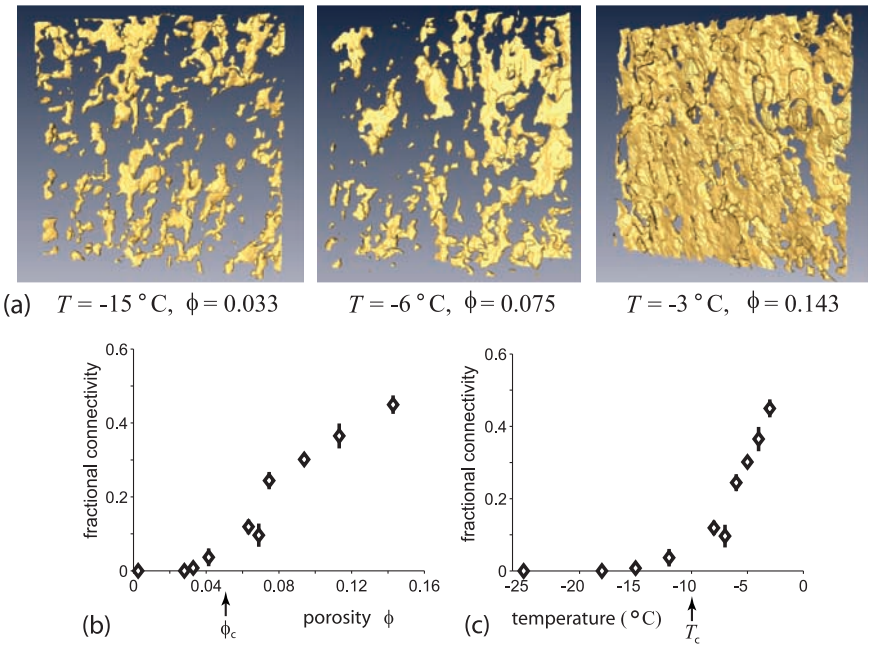

Figure 3. (a) X-ray CT volume rendering of brine layers within a lab-grown sea-ice single crystal with S = 9.3 ppt. The (non-collocated) 8 × 8 × 2 mm sub-volumes illustrate a pronounced change in the micro-scale morphology and connectivity of the brine inclusions during the step-wise warming cycle. (b) and (c) Vertical connectivity of inclusions over a cylinder of height 8 mm and diameter 21 mm. The fractional connectivity is the proportion of inclusions intersecting the upper surface which are also connected to the lower surface. The values $\phi_c \approx 0.05$ and $T_c \approx -10°$ C are the predicted [*Golden et al.*, 1998; *Petrich et al.*, 2006] bulk connectivity thresholds for sea ice with $S = 9.3$ ppt.

In Figure 2c, field data with ϕ in [0.055, 0.15], just above $\phi_c \approx 0.05$ [*Golden et al.*, 1998; *Petrich et al.*, 2006] are compared with (4), showing close agreement. A best fit for e of 1.94 was obtained from other data [*Ono and Kasai*, 1985].

[13] X-ray CT has provided new insight into small-scale, intra-crystalline brine layer connectivity. Figure 3a illustrates the thermal evolution of inclusion morphology and connectivity, the latter being quantified in Figures 3b and 3c [*Prodanovic et al.*, 2006]. Figure 3b provides the first direct observation of an onset in connectivity over this scale (≈1 cm). Consistent with percolation theory, this appears to occur at a lower porosity than the predicted threshold for bulk connectivity ($\phi_c \approx 0.05$). Notably, the thermal evolution of pore morphology in (a) is more complex than the classic model [*Thomas and Dieckmann*, 2003; *Weeks and Ackley*, 1986] (a transition from brine sheets to cylindrical to spheroidal inclusions) which underlies a range of porosity models [*Thomas and Dieckmann*, 2003; *Weeks and Ackley*, 1986]. These images provide insight into and constraints for more detailed modeling of micro-scale inclusion connectivity. A similar analysis of large-scale pore networks remains challenging, but is inherently reflected in the in situ permeability data.

[14] To model $k(\phi)$ over all porosities, we consider features of the brine phase present over the full range – some degree of connectivity, particularly on small scales, and self-similarity. The basic unit of sea ice microstructure is an ice grain surrounded by brine and ice, having substructure itself on smaller scales. Hierarchical, self-similar models of spheres or other grains surrounded by smaller spheres, and so on, with brine of conductivity σ_w in the pore spaces, have been used to describe the transport properties of sedimentary rocks [*Sen et al.*, 1981; *Wong et al.*, 1984]. Effective medium theory [*Sen et al.*, 1981; *Wong et al.*, 1984] gives Archie's law $\sigma = \sigma_w \phi^m$ as the conductivity of the model with exact results for the exponent m, such as $m = 3/2$ for spherical grains. The corresponding permeability exponent [*Wong et al.*, 1984] is $2m$, so that with k_0 as above and $m = 3/2$, the simplest hierarchical model yields

$$k(\phi) = 3\phi^3 \times 10^{-8} \text{ m}^2. \quad (5)$$

In Figure 4a the full in situ data set is compared to this theoretical prediction, with close agreement. From photomicrographs of marine sand microstructures [*Jackson et al.*, 1978] compacted platey sand appears the most similar to the cellular substructure of sea ice. In this case, $2m \approx 3.04$, which is closer to the best fit of 3.05 from our field data. For calcite aggregates and Fontainebleau sandstone, a cubic power law like (5) agrees closely with permeability data for porosities above about 10% [*Knackstedt and Cox*, 1995], with an exponent $2m \approx 3.05$ for Fontainebleau sandstone [*Bourbie and Zinszner*, 1985].

[15] In previous work [*Zhu et al.*, 2006] a two dimensional pipe network was developed to simulate fluid flow through a porous medium. For sea ice the cross-sectional areas A of the pipes are chosen from the lognormal distribution in (1), with $\langle A(\phi) \rangle$ as before and $\sigma^2 = 1$. The system was solved using a fast multigrid method. While the model compared well with lab data for $\phi > 0.15$, it overestimated $k(\phi)$ for $\phi < 0.15$ where percolation effects, which were ignored, become significant. In accordance with Figure 3b, here we introduce random disconnections so that

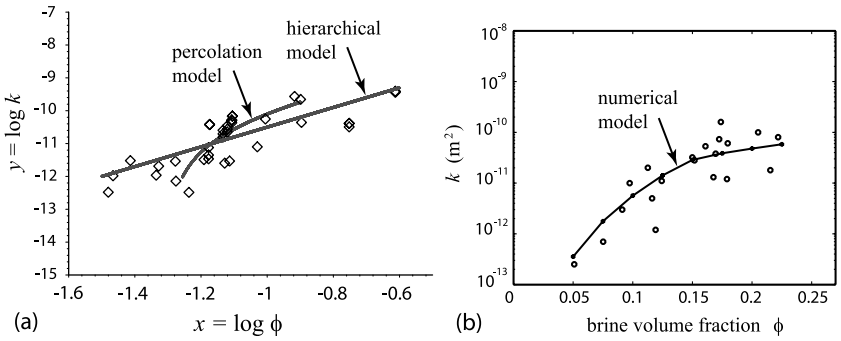

Figure 4. (a) Comparison of Arctic permeability data (37 data points) with our theoretical prediction in (5). In logarithmic variables the predicted line has the equation $y = 3\,x - 7.5$, while a best fit of the data yields $y = 3.05\,x - 7.50$. The lab data on artificially grown sea ice [*Freitag*, 1999] give a best fit of $y = 3.1\,x - 7.7$. (b) Comparison of lab data with numerical simulation.

the fluid network falls apart as ϕ decreases, and mostly so by $\phi_c \approx 0.05$. The results then agree well with the lab data, as shown in Figure 4b.

3. Conclusions

[16] The hierarchical model, characterized by the line in Figure 4a, provides perhaps the coarsest estimate of sea ice permeability which still captures the overall trend of the data for the full range of relevant porosities. The percolation model, as shown in Figure 4a, can be viewed as providing a higher order approximation for the permeability in the critical regime, which more accurately reflects our observations of brine connectivity. The numerical model is sufficiently robust to incorporate the results of further investigations of the brine microstructure and its evolution with temperature [*Pringle et al.*, 2006].

[17] Brine transport is central to a broad range of problems in the geophysics and biology of sea ice, yet fundamental studies have been lacking. Here we have developed a unified theory of the fluid permeability of sea ice and its dependence on microstructural evolution with temperature. The theory ties together different approaches to estimating effective composite behavior, and closely captures laboratory and Arctic field data. We have also made progress in CT imaging of sea-ice microstructure, quantifying the thermal evolution of pore connectivity and morphology at the (sub)granular scale, which in turn has informed the theoretical advances. Finally, we found that the fluid transport properties of sea ice bear a striking resemblance to those of some crustal rocks.

[18] Our work demonstrates how to link information about the micro-scale structure to macroscopic transport properties, which in turn constrain global-scale processes of climatological and biological importance. The results yield simple parameterizations of fluid transport through sea ice in terms of porosity ϕ, and therefore the state variables T and S, and can help to improve the representation of sea ice in climate, biogeochemical and geophysical models. Future studies will have to examine how these findings impact the simulation of heat and fluid flow through sea ice in large-scale models, the vast majority of which currently assume a constant salinity profile.

[19] **Acknowledgments.** We thank Stephen Ackley, Johannes Freitag, Chris Johnson, Victoria Lytle, Donald Perovich, Maša Prodanovic, Michael Shelley, and Po-zen Wong for helpful conversations. We also thank Patrick Cotter and Allen Sanderson for technical assistance. We are grateful for the support provided by the Division of Atmospheric Sciences and the Division of Mathematical Sciences at the US National Science Foundation (NSF), through grant DAS-0222171 in the Collaboration in Mathematical Geosciences (CMG) Program, and grant DMS-0537015. Amy Heaton gratefully acknowledges the support of the NSF Research Experiences for Undergraduates (REU) Program. This work was supported in part by a grant of HPC resources from the Arctic Region Supercomputing Center. CT data were analyzed with 3DMA software obtained from W. B. Lindquist et al., 2006, www.ams.sunysb.edu/~lindquis/3dma/3dma-rock/ 3dma-rock.html.

References

Berkowitz, B., and I. Balberg (1992), Percolation approach to the problem of hydraulic conductvity in porous media, *Transp. Porous Media*, *9*, 275–286.

Bock, C., and H. Eicken (2005), A magnetic resonance study of temperature-dependent microstructural evolution and self-diffusion of water in Arctic first-year sea ice, *Ann. Glaciol.*, *40*, 179–184.

Bourbie, T., and B. Zinszner (1985), Hydraulic and acoustic properties as a function of porosity in Fontainebleau sandstone, *J. Geophys. Res.*, *90*, 11,524–11,532.

Eicken, H., T. C. Grenfell, D. K. Perovich, J. A. Richter-Menge, and K. Frey (2004), Hydraulic controls of summer Arctic pack ice albedo, *J. Geophys. Res.*, *109*, C08007, doi:10.1029/2003JC001989.

Freitag, J. (1999), The hydraulic properties of Arctic sea ice: Implications for the small-scale particle transport (in German), *Ber. Polarforsch.*, *325*, 150 pp.

Freitag, J., and H. Eicken (2004), Meltwater circulation and permeability of Arctic summer sea ice derived from hydrological field experiments, *J. Glaciol.*, *49*, 349–358.

Friedman, A. P., and N. A. Seaton (1998), Critical path analysis of the relationship between permeability and electrical conductivity of three-dimensional pore networks, *Water Resour. Res.*, *34*, 1703–1710.

Fritsen, C. H., V. I. Lytle, S. F. Ackley, and C. W. Sullivan (1994), Autumn bloom of Antarctic pack-ice algae, *Science*, *266*, 782–784.

Golden, K. (1990), Convexty and exponent inequalities for conduction near percolation, *Phys. Rev. Lett.*, *65*, 2923–2926.

Golden, K. M., and S. M. Kozlov (1999), Critical path analysis of transport in highly disordered random media, in *Homogenization: Serguei Kozlov Memorial Volume*, edited by V. Berdichevsky, V. Jikov, and G. Papanicolaou, pp. 21–34, World Sci., Hackensack, N. J.

Golden, K. M., S. F. Ackley, and V. I. Lytle (1998), The percolation phase transition in sea ice, *Science*, *282*, 2238–2241.

Golden, K. M., A. L. Heaton, H. Eicken, and V. I. Lytle (2006), Void bounds for fluid transport in sea ice, *Mech. Mater.*, *38*, 801–817.

Halperin, B. I., S. Feng, and P. N. Sen (1985), Differences between lattice and continuum percolation transport exponents, *Phys. Rev. Lett.*, *54*, 2391–2394.

Jackson, P. D., D. T. Smith, and P. N. Stanford (1978), Resistivity-porosity-particle shape relationships for marine sands, *Geophysics*, *43*, 1250–1268.

Knackstedt, M. A., and S. F. Cox (1995), Percolation and pore geometry of crustal rocks, *Phys. Rev. E*, *51*, R5181–R5184.

Kusy, R. P., and D. T. Turner (1971), Electrical resistivity of a polymeric insulator containing segregated metallic particles, *Nature*, *229*, 58–59.

Oertling, A. B., and R. G. Watts (2004), Growth of and brine drainage from NaCl-H_2O freezing: A simulation of young sea ice, *J. Geophys. Res.*, *109*, C04013, doi:10.1029/2001JC001109.

Ono, N., and T. Kasai (1985), Surface layer salinity of young sea ice, *Ann. Glaciol.*, *6*, 298–299.

Perovich, D. K., and A. J. Gow (1996), A quantitative description of sea ice inclusions, *J. Geophys. Res.*, *101*, 18,327–18,343.

Petrich, C., P. J. Langhorne, and Z. F. Sun (2006), Modelling the interrelationships between permeability, effective porosity and total porosity in sea ice, *Cold Reg. Sci. Technol.*, *44*, 131–144.

Pringle, D., J. Miner, R. Glantz, M. Hilpert, and H. Eicken (2006), Temperature-dependent pore space of sea ice: X-ray computed-tomography and dual model network analysis, *Eos Trans. AGU*, *87*(52), Fall Meet. Suppl., Abstract H51F–0545.

Prodanović, M., W. B. Lindquist, and R. S. Seright (2006), Porous structure and fluid partitioning in polyethylene cores from 3D X-ray microtomographic imaging, *J. Colloid Interface Sci.*, *298*, 282–297.

Sen, P. N., C. Scala, and M. H. Cohen (1981), A self-similar model for sedimentary rocks with application to the dielectric constant of fused glass beads, *Geophysics*, *46*, 781–795.

Serreze, M. C., M. M. Holland, and J. Stroeve (2007), Perspectives on the Arctic's shrinking sea-ice cover, *Science*, *315*, 1533–1536.

Thomas, D. N., and G. S. Dieckmann (2002), Antarctic sea ice: A habitat for extremophiles, *Science*, *295*, 641–644.

Thomas, D. N., , and G. S. Dieckmann (Eds.) (2003), *Sea Ice: An Introduction to Its Physics, Chemistry, Biology and Geology*, Blackwell, Oxford, U. K.

Torquato, S. (2002), *Random Heterogeneous Materials: Microstructure and Macroscopic Properties*, Springer, New York.

Torquato, S., and D. C. Pham (2004), Optimal bounds on the trapping constant and permeability of porous media, *Phys. Rev. Lett.*, *92*, 255505, doi:10.1103/PhysRevLett.92.255505.

Weeks, W. F., and S. F. Ackley (1986), The growth, structure and properties of sea ice, in *The Geophysics of Sea Ice*, edited by N. Untersteiner, pp. 9–164, Plenum, New York.

Wettlaufer, J. S., M. G. Worster, and H. E. Huppert (1997), Natural convection during solidification of an alloy from above with application to the evolution of sea ice, *J. Fluid Mech.*, *344*, 291–316.

Wong, P., J. Koplick, and J. P. Tomanic (1984), Conductivity and permeability of rocks, *Phys. Rev. B*, *30*, 6606–6614.

Zhu, J., A. Jabini, K. M. Golden, H. Eicken, and M. Morris (2006), A network model for fluid transport in sea ice, *Ann. Glaciol.*, *44*, 129–133.

H. Eicken and J. Miner, Geophysical Institute, University of Alaska Fairbanks, P.O. Box 757320, Fairbanks, AK 99775, USA.

K. M. Golden, A. L. Heaton, and J. Zhu, University of Utah, Department of Mathematics, 155 S 1400 E RM 233, Salt Lake City, UT 84112-0090, USA.

D. J. Pringle, Arctic Region Supercomputing Center, University of Alaska Fairbanks, P.O. Box 756020, Fairbanks, AK 99775, USA.